Title

^{18}F-Fluorosulfate for PET imaging of the sodium/iodide symporter: synthesis and biological evaluation *in vitro* and *in vivo*

Running Title

^{18}F-SO$_3$F$^-$ for PET imaging of NIS

Authors

Alex Khoshnevisan[1], Krisanat Chuamsaamarkkee[1], Mehdi Boudjemeline[1,†], Alex Jackson[2], Gareth E. Smith[2], Antony D. Gee[1], Gilbert O. Fruhwirth[1], Philip J. Blower[1*]

Affiliations

1 - King's College London, Division of Imaging Sciences and Biomedical Engineering, 4th Floor Lambeth Wing, St. Thomas' Hospital, London SE1 7EH, United Kingdom

2 – GE Healthcare, The Grove Centre, White Lion Road, Amersham, United Kingdom

†Current address: McGill University, McConnell Brain Imaging Centre, Montreal Neurological Institute, Montreal H3A 2B4, Canada

Corresponding Author Details

*Prof. Philip J. Blower; Address: King's College London, Division of Imaging Sciences and Biomedical Engineering, 4th Floor Lambeth Wing, St. Thomas' Hospital, London SE1 7EH, United Kingdom; Tel: +44(0)2071889513; Email: philip.blower@kcl.ac.uk

First Author Details

Mr. Alex Khoshnevisan; Address: King's College London, Division of Imaging Sciences and Biomedical Engineering, 4th Floor Lambeth Wing, St. Thomas' Hospital, London SE1 7EH, United Kingdom; Tel: +44(0)2071888376; Email: alex.khoshnevisan@kcl.ac.uk, PhD Student

Word count: 5000

ABSTRACT

Purpose: Anion transport by the human sodium/iodide symporter (hNIS) is an established target for molecular imaging and radionuclide therapy. Current radiotracers for positron emission tomography (PET) of hNIS expression are limited to $^{124}I^-$ and $^{18}F-BF_4^-$. We sought new ^{18}F-labeled hNIS substrates offering higher specific activity, higher affinity and simpler radiochemical synthesis than $^{18}F-BF_4^-$.

Methods: The ability of a range of anions, some containing fluorine, to block $^{99m}TcO_4^-$ uptake in hNIS-expressing cells was measured. SO_3F^- emerged as a promising candidate. $^{18}F-SO_3F^-$ was synthesized by reaction of $^{18}F^-$ with SO_3-pyridine complex in MeCN and purified using alumina and quaternary methyl ammonium (QMA) solid phase extraction cartridges. Chemical and radiochemical purity (RCP) and serum stability were determined by radiochromatography. Radiotracer uptake and efflux in hNIS-transduced HCT116-C19 cells and the hNIS-negative parent cell line were evaluated *in vitro* in the presence and absence of a known competitive inhibitor (NaClO$_4$). PET/CT (CT = computed tomography) imaging and *ex vivo* biodistribution measurement were conducted in BALB/c mice, with and without NaClO$_4$ inhibition.

Results: Fluorosulfate was identified as a potent inhibitor of $^{99m}TcO_4^-$ uptake via hNIS *in vitro* (IC$_{50}$ 0.55-0.56 µM, cf. BF$_4^-$ 0.29-4.5, TcO$_4^-$ 0.07, I$^-$ 2.7-4.7 µM). Radiolabeling to produce $^{18}F-SO_3F^-$ was simple and afforded high RCP, suitable for biological evaluation (RCP > 95%, decay corrected radiochemical yield (RCY) = 31.6%, specific activity $\geq$ 48.5 GBq/µmol). Specific, blockable hNIS-mediated uptake in HCT116-C19 cells was observed *in vitro*, and PET/CT imaging in normal mice showed uptake in thyroid, salivary glands (%ID/g at 30 min: 563 $\pm$ 140 and 32 $\pm$ 9 respectively) and stomach (%ID/g at 90 min: 68 $\pm$ 21).

Conclusions: Fluorosulfate is a high-affinity hNIS substrate. $^{18}F\text{-}SO_3F^-$ is easily synthesized in high yield and very high specific activity and is a promising candidate for pre-clinical and clinical PET imaging of hNIS expression and thyroid-related disease; it is the first example of *in vivo* PET imaging with a tracer containing a S-^{18}F bond.

Keywords

Human sodium/iodide symporter (SC5A5); fluorosulfate; fluorine-18; PET; thyroid

INTRODUCTION

The sodium/iodide symporter (NIS) is capable of intracellular concentration of certain small anions against their electrochemical gradient, and is biologically important for accumulating iodide in thyroid follicles for synthesis of thyroid hormones. Several radioactive substrates of human NIS (hNIS; SC5A5) have been used for radionuclide therapy ($^{131}I^-$) and SPECT ($^{131/123}I^-$, $^{99m}TcO_4^-$) and PET ($^{124}I^-$) imaging of thyroid-related disorders (*1*). Other radioactive substrates currently being evaluated as next-generation radiopharmaceuticals for these purposes include $^{186/188}ReO_4^-$ for therapy (*2,3*) and ^{18}F-BF_4^- for PET (*4,5*). ^{18}F-BF_4^- is the prototype ^{18}F-labeled NIS tracer, offering the advantages of moderate half-life, excellent imaging characteristics associated with a high yield of low-energy positrons, minimal undesirable photon emissions, low absorbed radiation dose (*6*) and wide availability. With these characteristics, it is expected to offer superior imaging compared to SPECT with $^{123/131}I$ and PET with ^{124}I. However, among the known substrates of NIS it has mid-ranking affinity (IC_{50} of 1.2 μM for inhibition of $^{124}I^-$ uptake, c.f. IC_{50} of ClO_4^- is 0.1 μM in the same assay (*7*)), and chemical constraints during synthesis lead to low specific activity (*4,8*). Consequently, alternative ^{18}F-labeled NIS substrates that overcome these limitations are desirable.

A search of the literature for alternative fluorine-containing NIS substrates reveals several that merit further investigation. Both SO_3F^- and $PO_2F_2^-$ are known to inhibit radioiodide uptake in mouse thyroid (*9*), yet in quantitative terms their effectiveness as substrates or inhibitors of hNIS is unknown. PF_6^- is a highly potent inhibitor of rat NIS (IC_{50} = 15 nM (*10*)). We therefore performed a preliminary comparison of their ability to inhibit hNIS using uptake in hNIS expressing cells with ^{99m}Tc-pertechnetate as a probe. From this survey we selected SO_3F^- based on its high affinity and potentially straightforward radiolabeling.

Here we report a comparison of fluorine-containing anions with other known hNIS substrates and, for the first time, a simple method for radiosynthesis of ^{18}F-SO$_3$F$^-$ and its biological evaluation in hNIS-expressing cells and *in vivo* in mice.

MATERIALS AND METHODS

General

Unless otherwise stated, all chemicals were from Sigma Aldrich (Gillingham, UK). Ammonium difluorophosphate was synthesized as previously described (*11*) (NMR data in Supplementary Figs. 1 and 2). ^{18}F$^-$ was produced as previously described (*4*). ^{99m}TcO$_4^-$ was obtained from Guy's Hospital Radiopharmacy (London, UK) and used ~4.5 h after elution (24 h between elutions). Animal experiments were performed under a UK Home Office licence following UK Research Councils' and Medical Research Charities' guidance on Responsibility in the Use of Animals in Bioscience Research, as approved by the local institutional ethics committee. Inhibitory potency was assessed by pertechnetate uptake blockade, using two different cell lines expressing hNIS: (i) a virally infected breast adenocarcinoma cell line stably expressing hNIS (*12*): MTLn3E.Δ34 CXCR4-eGFP hNIS-tag-RFP cells, hereafter referred to as 3E.Δ-NIS cells), and (ii) a human colon carcinoma cell line transfected to stably express hNIS under selection pressure (HCT116-hNIS-C19 (*5*)). Parental cell lines served as negative controls. HCT116 was also used to study the cellular uptake of ^{18}F-SO$_3$F$^-$ in the absence of hNIS. Ionic volumes were either taken directly from literature (*13*), or calculated by the method described therein from crystallographic data (PO$_2$F$_2^-$ (*14*); TcO$_4^-$ (*15,16*)).

Optimized radiosynthesis

The following procedure was arrived at after optimization of reaction time, temperature and conditions. Solutions of K_2CO_3 (5.2 mg) in H_2O (0.4 mL) and of K[2.2.2] (14.2 mg) in MeCN (1.1 mL) were prepared. K_2CO_3 solution (0.2 mL) was added to the K[2.2.2] solution to form QMA eluent. ^{18}F-fluoride was trapped from ^{18}O-H_2O on a QMA cartridge (preconditioned with $NaHCO_3$ (10 mL), H_2O (10 mL)), eluted with QMA eluent (0.9 mL), dried by azeotropic distillation of MeCN (0.4 mL) under a N_2 stream at 110°C for 5 min then twice further at 95°C. SO_3-pyridine complex (5 mg) in MeCN (1 mL) was then added followed by heating to 80°C for 10 min. The reaction was quenched with H_2O (2 mL) and the solution passed through a neutral alumina cartridge (preconditioned with H_2O (20 mL) and air (10 mL)) and a QMA cartridge (preconditioned with 1M NaCl (5 mL), H_2O (10 mL)). The QMA was washed with H_2O (4 mL) and the product eluted with 0.9% NaCl (0.4 mL) ready for biological evaluation. RadioTLC (R_f values: $SO_3F^- = 0.43$, $F^- = 0$) details: neutral alumina stationary phase (Macherey-Nagel, 10 x 80 mm, Polygram® ALOX N/UV$_{254}$), methanol mobile phase; LabLogic Mini-Scan^{TM} scanner with β^+ probe (LabLogic B-FC-3600). Radiochemical identity, purity, specific activity and sulfate concentration were established by ion chromatography (IC, Metrohm 930 Compact IC Flex) with in-line conductimetric and gamma detectors, using a Shodex IC I-524A column (4.6 x 100 mm) eluted with aqueous 2.3 mM phthalic acid and 2.3 mM tris(hydroxymethyl)aminomethane (pH 5.0), flow rate 1.5 mL/min, column temperature 30°C; limit of detection was 894 ng/mL for KSO_3F. Pyridine was determined by HPLC (Agilent 1200 series, UV/VIS 210 nm; Agilent Zorbax 300-SCX column eluted with 0.2 M sodium phosphate (pH 3), 1.0 mL/min). K[2.2.2] concentration was determined as described previously (*17*).

^{99m}TcO$_4^-$ uptake inhibition assay (HCT116-hNIS-C19 cells)

HCT116-hNIS-C19 cells seeded in 12-well plates (5 x 10^5 cells/well) were incubated with 5% CO_2 at 37°C for 24 h, washed twice with HBSS before incubation with the chosen inhibitory anion in HBSS (700 µL concentration between 1 x 10^{-2} and 1 x 10^{-13} M, n = 3 each) for 30 min. $^{99m}TcO_4^-$ (0.1 MBq, ~37 pM) in HBSS (50 µL) was added followed by 30 min incubation. The medium was removed and cells were washed with HBSS (750 µL) and extracted with 1M NaOH (750 µL). Bound and unbound radioactivity were gamma counted. IC_{50} values were determined by least squares fitting of a sigmoidal curve (GraphPad Prism v5.03).

$^{99m}TcO_4^-$ uptake inhibition assay (3E.Δ-NIS cells)

3E.Δ-NIS cells seeded in 6-well plates were incubated as above for 12 h, washed with PBS (1 mL), incubated with PBS (1 mL) containing the inhibitor (range 1 x 10^{-11} to 5 x 10^{-4} M, n = 3 each) and 50 kBq/mL of $^{99m}TcO_4^-$ (~14 pM) for 30 min, washed twice with PBS (1.4 mL), trypsinized (900 µL of 250 USP/mg in PBS) at 37°C during 5 min, resuspended in PBS (250 µL) and centrifuged. Cell-bound and combined media and washings were gamma counted. Data were fitted to sigmoidal curves using Microcal Origin v8.0.

Stability studies

^{18}F-SO_3F^- was incubated in 0.9% NaCl or 50 mM glycine/HCl buffer (pH 3.0) at 25°C for 4 h, and analysed by IC and TLC as described above. ^{18}F-SO_3F^- (~25 MBq) in 0.9% NaCl (100 µL) was incubated with human serum (1 mL) at 37°C for 4 h. Hourly samples (100 µL) were mixed with ethanol (100 µL) to precipitate proteins, centrifuged and supernatants analyzed by TLC.

[^{18}F]SO_3F^- cell binding study

HCT116-hNIS-C19 or HCT116 cells seeded in 6-well plates (1×10^6 cells/well) were incubated as above for 24 h, washed twice with HBSS, and incubated in HBSS (950 μL) with or without $NaClO_4$ (20 μM) for 30 min. $^{18}F\text{-}SO_3F^-$ (0.1 MBq) in HBSS (50 μL) was then added followed by incubation for 30 min (in triplicate). Cells were washed with HBSS (1 mL), extracted with 1M NaOH (1 mL) and the cell extract and medium/washings gamma counted. Intracellular to extracellular concentration ratios were estimated using a mean cell diameter of 18.4 μm (*18*).

$^{18}F\text{-}SO_3F^-$ self-inhibition

HCT116-hNIS-C19 cells seeded in 12-well plates (5×10^5 /well) were incubated as above for 24 h, washed twice with HBSS, incubated with KSO_3F (range 1×10^{-2} to 10^{-12} M, n = 3 each) in HBSS (700 μL) for 30 min. $^{18}F\text{-}SO_3F^-$ (0.1 MBq) in HBSS (50 μL) was then added and incubated for 30 min. Cells were washed and counted and IC_{50} determined as above.

$^{18}F\text{-}SO_3F^-$ cell efflux

HCT116-hNIS-C19 cells were prepared as for self-inhibition experiment above, incubated with $^{18}F\text{-}SO_3F^-$ (0.1 MBq) in HBSS (750 μL) for 60 min, and washed with cold HBSS (750 μL) before adding fresh tracer-free medium. Cells and medium were sampled and gamma counted as described above.

PET imaging

Female BALB/c mice (4 - 8 weeks) were given either $NaClO_4$ (250 mg/kg intraperitoneal injection as a competitive substrate for inhibitive effect) in 0.9% NaCl or an equal volume of 0.9% NaCl (sham inhibitor). One hour later $^{18}F\text{-}SO_3F^-$ (~5 MBq in 0.9% NaCl, 150 μL) was injected (tail vein) under anesthesia maintained using 1.5 - 2% isoflurane gas (Isocare®, in O_2

(Animalcare, York, UK)). The mouse was then transferred to the scanner bed maintaining anesthesia, bed warming and vital signs monitoring. Dynamic PET was acquired for 2 h (starting < 1 min after tracer injection) on the nanoScan-PET/CT (Mediso, Hungary) in list mode using a 400-600 keV energy window, coincidence relation 1:3, followed by CT (55 keV X-ray, exposure 1000 ms, 360 projections, pitch 1). PET data were processed with Tera-tomo® software (supplied with the system) with attenuation, scatter and dead-time corrections, re-binned and reconstructed into a series of 5 min frames for the first 30 min and 30 min frames thereafter. VivoQuant© (InviCro, Boston, USA) software was used to view and quantify data. Regions of interest (ROIs) were manually drawn over thyroid, salivary glands, stomach, bladder, left ventricle (for blood), and muscle at a threshold of 10% of the maximum count to define the edges of the ROI. Time-activity curves were generated and expressed as percentage injected dose (%ID, with whole body ROI activity, excluding tail, as the injected dose) and percentage injected dose per *ex vivo* weight of organ (%ID/g).

Ex vivo biodistribution

At 2.25 h post-injection, scanned mice were culled by cervical dislocation and tissues were harvested, weighed and gamma counted (1282 Compugamma; LKB, channels 175-220). Data were presented as %ID/g (ID = total activity of all body parts including carcass, and any urine excreted at the time of culling, but excluding the tail). Calculations requiring thyroid weight were conducted using a standard weight of 3.6 mg (*4,19*).

RESULTS

^{99m}TcO$_4^-$ uptake inhibition assay

The half-maximal inhibitory concentrations (IC_{50}) for the anions assessed for their ability to block $^{99m}TcO_4^-$ or $^{18}F\text{-}BF_4^-$ uptake via hNIS are detailed in SI (Supplementary Table 1, which also includes comparable literature data (*5,7,8,10,20*)). The potency was in the order $SCN^- < PO_2F_2^- < I^- < BF_4^- \approx SO_3F^- < ReO_4^- < TcO_4^- < PF_6^-$, which roughly parallels the increase in ionic volume (Fig. 1). Literature data on inhibitory potency and affinity of anions are not comprehensive but where available are broadly consistent with our results. Of the fluorine-containing substrates, PF_6^- (IC_{50} 21 nM) was the most potent but SO_3F^- had potency (IC_{50} 0.56 µM) comparable to BF_4^- and better than iodide (IC_{50} >2.7 mM), and is more likely to be amenable to simple radiosynthesis than BF_4^-. SO_3F^- was therefore selected for development of a new PET tracer.

Radiosynthesis of $^{18}F\text{-}SO_3F^-$

Reaction of K[2.2.2]/$^{18}F\text{-}KF$ with SO_3-pyridine complex (Fig. 2) afforded $^{18}F\text{-}SO_3F^-$. Varying the reaction conditions (Supplementary Table 2) led to crude RCY values as high as 65%. Passage through an alumina column removed unreacted $^{18}F^-$, and the eluted product could be trapped on a QMA cartridge allowing washing to remove pyridine and K[2.2.2], and eluted in 0.9% NaCl (RCY 31.6 ± 9.5% (n = 3, decay corrected) and RCP 96 ± 1% (always ≥ 95%)). The total synthesis time from end of bombardment was less than 1 hour. The identity of the product was confirmed by IC with co-injection of authentic SO_3F^- as a reference (Fig. 3). With a starting radioactivity of ~750 MBq, a specific activity of ≥ 48.5 ± 13.4 GBq/µmol (n = 3) was obtained in a volume of 0.4 mL. The product contained residual pyridine (1.4 ± 1 µg/mL, 0.56 µg total), K[2.2.2] (< 6.25 µg/mL, < 2.5 µg total) and SO_4^{2-} (302 ± 26 µg/mL, 120.7 µg total), and had a pH of 7.

In vitro uptake, efflux and self-inhibition of $^{18}F\text{-}SO_3F^-$

Significant uptake of the radiotracer in hNIS-expressing HCT116-C19 cells was observed and was blocked by $NaClO_4$ (Fig. 4). No uptake occurred in the parental cell line HCT116 (which does not express hNIS), with or without $NaClO_4$. Uptake and efflux from the cells both reached equilibrium within 80 min (Supplementary Figs. 3 and 4). Uptake at equilibrium was consistent with an intracellular-to-extracellular $^{18}F\text{-}SO_3F^-$ concentration ratio of 76:1. Under identical conditions the ratio for $^{99m}TcO_4^-$ was 44:1, and that for $^{18}F\text{-}BF_4^-$ was 24:1 (calculated from data obtained during this and other studies (7) respectively). Inhibition of $^{18}F\text{-}SO_3F^-$ uptake in HCT116-C19 cells by KSO_3F occurred with an IC_{50} of 1.6 μM (Fig. 5).

Serum stability

IC and TLC of the tracer both as formulated and under acidic conditions (pH 3.0) was unchanged (RCP > 95%) after 4 h at room temperature. Similarly, the RCP was > 95% after 4 h incubation (37°C) in serum, as assessed by TLC of the supernatant after protein precipitation with ethanol (no significant radioactivity was associated with the protein pellet). These data are summarised in Supplementary Table 3.

PET/CT imaging

PET/CT of $^{18}F\text{-}SO_3F^-$ (Fig. 6) in normal mice revealed prominent uptake in thyroid, stomach and salivary glands, that was suppressed in the perchlorate-treated mice. Time-activity curves (%ID/g, Supplementary Figs. 5 and 6; %ID, Supplementary Figs. 7 and 8) over a 2 h imaging period showed thyroid and salivary gland uptake plateauing around 30-45 min (563 ± 140 and 32 ± 9 %ID/g at 30 min respectively), with stomach uptake plateauing around 90 min (68 ± 21 %ID/g at 90 min). Bone uptake first became detectable at 30 min and increased to 3 ± 1 %ID/g by 60 min.

Ex vivo **biodistribution in mice**

At 2.25 h post-injection, uptake of ^{18}F-SO$_3$F$^-$ consistent with the PET scans was observed in thyroid (144 ± 71 %ID/g), stomach (59 ± 10 %ID/g) and salivary glands (18 ± 4 %ID/g); uptake in these organs was reduced to 4.3 ± 4.6 , 3.0 ± 1.7 and 2.6 ± 1.7 %ID/g respectively, in mice administered NaClO$_4$ (Fig. 6, and shown as SUV in Supplementary Fig. 9). Radioactivity observed in the bladder (15 ± 14 %ID/g) indicates renal excretion. A small amount of radioactivity uptake in bone (17 ± 3 %ID/g) occurred and was not blocked by perchlorate, suggesting that some defluorination occurs over two hours that was not seen during incubation in serum.

DISCUSSION

Evaluation of the inhibitory potency of fluorosulfate on hNIS both confirmed its previously-suggested (*9*) status as a potent inhibitor/competitive substrate, with greater potency than I$^-$ and possibly BF$_4^-$. The range of IC$_{50}$ values found for both BF$_4^-$ (currently undergoing evaluation as a clinical PET tracer for hNIS) and SO$_3$F$^-$, is lower than that found for iodide (Fig. 1 and Supplementary Table 1). Although inhibitory potency may not be directly indicative of ability to reach a high intracellular-extracellular concentration gradient in hNIS expressing cells (which is the key requirement of a good PET tracer for hNIS), the data do suggest that ^{18}F-SO$_3$F$^-$ would be a high affinity NIS tracer. Analysis of the ionic volume (*13*) in relation to the IC$_{50}$ of several anions against radioiodide (*10*), ^{99m}TcO$_4^-$ or ^{18}F-BF$_4^-$ uptake suggests that larger anions are more effective inhibitors of hNIS (Fig. 1). Accordingly, PF$_6^-$ was found to be the most potent inhibitor examined (IC$_{50}$ 21 nM). However, in contrast to other known fluorine-containing NIS

inhibitors, such as PF_6^- and BF_4^-, SO_3F^- has the advantage of bearing a single fluorine atom. Thus, no-carrier-added radiolabeling of SO_3F^- would yield a specific activity limited only by the fluorine-18 source. We therefore chose $^{18}F\text{-}SO_3F^-$ as a target for development of a new fluorine-18-labeled hNIS tracer.

Our strategy for synthesising $^{18}F\text{-}SO_3F^-$ involved utilizing a Lewis acid-base sulfur trioxide-pyridine adduct, which is readily available in pure form. Radiolabeling proceeded via displacement of the pyridine by $^{18}F^-$ followed by quenching with water to hydrolyse residual starting material to sulfate. Formation of $^{18}F\text{-}SO_3F^-$, confirmed by TLC and IC, was observed under all reaction conditions. More basic conditions with elevated temperature and precursor concentration enhanced incorporation of $^{18}F^-$ into $^{18}F\text{-}SO_3F^-$. Further optimization may lead to improved yields, e.g. using alternatives to pyridine as the Lewis base in the precursor complex.

Purification using sequential alumina and QMA cartridges yielded $^{18}F\text{-}SO_3F^-$ in saline, conveniently suitable for biological use, with high radiochemical and chemical purity. Residual pyridine and K[2.2.2] in the final product are within acceptance limits set out in the British Pharmacopoeia. The sulfate concentration resulting from precursor hydrolysis is also safe considering that $MgSO_4$ can be administered in gram quantities intravenously with minimal side effects (*21*). The specific activity of $^{18}F\text{-}SO_3F^-$ ($\geq$ 48.5 GBq/µmol) is significantly higher than that reported for $^{18}F\text{-}BF_4^-$ (1 (*4*), 5 (*7*) or up to 8.8 (*22*) GBq/µmol) as there is no ^{19}F naturally present in the precursor. The specific activity is therefore limited only by that of the initial $^{18}F^-$ and the purity of the other reagents. The method is amenable to automation, and modification of the radiosynthesis to conform to Good Manufacturing Practices should be straightforward. The high specific activity minimizes the pharmacological dose administered.

Assessing the biological activity of ^{18}F-SO$_3$F$^-$ *in vitro* in a hNIS-expressing cell line confirmed specific NIS-mediated uptake that was absent both in hNIS-negative cells and in the presence of competitive inhibition by perchlorate. Uptake and efflux showed kinetics (equilibrium reached in under 80 min) appropriate for *in vivo* use. The specific activity of the ^{18}F-SO$_3$F$^-$ is very high and more than sufficient to realise the potential benefit of the high affinity: assuming an injected activity of ~10 MBq for a PET/CT scan in a mouse with an extracellular fluid volume of 5 mL, the *in vivo* concentration of $^{18/19}$F-SO$_3$F$^-$ will be < 41 nM, well below the concentration at which *in vitro* inhibition is observed (Fig. 5). As well as a high affinity of ^{18}F-SO$_3$F$^-$ for hNIS demonstrated by the IC$_{50}$ of 0.56 μM, the plateau intracellular-to-extracellular radioactivity concentration ratio *in vitro* (76:1) was higher than for either ^{99m}Tc-pertechetate (44:1) or ^{18}F-BF$_4$$^-$ (24:1), suggesting that, other pharmacokinetic features being similar, a higher target-to-background ratio might be expected in PET images.

PET/CT imaging of ^{18}F-SO$_3$F$^-$ in normal mice during the first hour post-injection revealed uptake at sites known to express NIS. This signal was abolished by co-administration of NaClO$_4$. This shows that the tracer is an excellent substrate for mouse NIS as well as hNIS. Maxima were reached in both thyroid uptake (Supplementary Fig. 5) and thyroid to muscle (as a background reference) uptake ratio (Supplementary Fig. 10) after 30 min, confirming this as the ideal imaging time point. While barely detectable at 30 min (%ID/g <1% of that in thyroid), there was increasing signal in the bones at later time points, both in PET images (Supplementary Figs. 11-13) and in the *ex vivo* biodistribution data. While the *in vivo* hydrolysis of fluorosulfate to sulfate and fluoride is known (*23*), it is unlikely to hamper the utility of the tracer in hNIS imaging because uptake at sites of NIS expression reaches its maximum long before bone uptake is significant.

CONCLUSION

Several fluorine-containing anions are potent hNIS inhibitors. Among them SO_3F^- is a hNIS inhibitor containing a single fluorine atom and has an inhibitory potency similar to or greater than that of tetrafluoroborate, and greater than iodide. It is readily synthesized in ^{18}F-radiolabeled form in high yield, RCP and specific activity. ^{18}F-SO_3F^- shows NIS-specific uptake *in vitro* and *in vivo* and is an excellent candidate for further preclinical and clinical evaluations as a hNIS PET imaging agent for application in thyroid-related disease and hNIS reporter gene imaging. To our knowledge, this work is the first example of imaging *in vivo* by PET/CT using a tracer with a S-^{18}F bond. The simplicity of ^{18}F-SO_3F^- synthesis, and its adequate *in vivo* stability, suggest that "inorganic" ^{18}F-radiopharmaceutical synthesis (*24*) whereby atoms other than carbon, such as aluminum, silicon, boron, and now sulfur (*25*), serve as binding sites for ^{18}F, deserves further attention.

Disclosure

ACKNOWLEDGEMENTS

Authors Contributions

PJB conceived the study, secured funding and contributed to its design and coordination. GOF and MB contributed data on pertechnetate uptake inhibition. AK developed the fluorosulfate radiolabelling, radioanalytical methods and performed *in vitro* and serum stability studies. KC and AK performed the *in vivo* experiments. AJ, GS and ADG contributed to study design. The manuscript was drafted by AK and PJB and edited by all other authors. All authors have read and approved the final manuscript.

REFERENCES

1. Ahn B-C. Sodium iodide symporter for nuclear molecular imaging and gene therapy: from bedside to bench and back. *Theranostics.* 2012;2:392–402.

2. Riese CGU, Seitz S, Schipper ML, Behr TM. Effective treatment of pancreatic neuroendocrine tumours transfected with the sodium iodide symporter gene by [186]Re-perrhenate in mice. *Eur J Nucl Med Mol Imaging.* 2009;36:1767–1773.

3. Dadachova E, Bouzahzah B, Zuckier LS, Pestell RG. Rhenium-188 as an alternative to iodine-131 for treatment of breast tumors expressing the sodium/iodide symporter (NIS). *Nucl Med Biol.* 2002;29:13–18.

4. Jauregui-Osoro M, Sunassee K, Weeks AJ, et al. Synthesis and biological evaluation of [18F]tetrafluoroborate: a PET imaging agent for thyroid disease and reporter gene imaging of the sodium/iodide symporter. *Eur J Nucl Med Mol Imaging.* 2010;37:2108–2116.

5. Weeks AJ, Jauregui-Osoro M, Cleij M, Blower JE, Ballinger JR, Blower PJ. Evaluation of [18F]-tetrafluoroborate as a potential PET imaging agent for the human sodium/iodide symporter in a new colon carcinoma cell line, HCT116, expressing hNIS. *Nucl Med Commun.* 2011;32:98–105.

6. Marti-Climent JM, Collantes M, Jauregui-Osoro M, et al. Radiation dosimetry and biodistribution in non-human primates of the sodium/iodide PET ligand [18F]-tetrafluoroborate. *EJNMMI Res.* 2015;5:70

7. Tonacchera M, Pinchera A, Dimida A, et al. Relative potencies and additivity of perchlorate, thiocyanate, nitrate, and iodide on the inhibition of radioactive iodide uptake by the human sodium iodide symporter. *Thyroid.* 2004;14:1012–1019.

8. Khoshnevisan A, Jauregui-Osoro M, Shaw K, et al. [^{18}F]tetrafluoroborate as a PET tracer for the sodium/iodide symporter: the importance of specific activity. *EJNMMI Res.* 2016;6:34

9. Anbar M, Guttmann S, Lewitus Z. Effect of monofluorosulphonate, difluorophosphate and fluoroborate ions on the iodine uptake of the thyroid gland. *Nature.* 1959;183:1517–1518.

10. Waltz F, Pillette L, Ambroise Y. A nonradioactive iodide uptake assay for sodium iodide symporter function. *Anal Biochem.* 2010;396:91–95.

11. Lange W, Booth HS, Kendall F. Ammonium difluophosphate. In: Fernelius WC, editor. *Inorg Synth* John Wiley & Sons, Inc.; 1946 p. 157–158.

12. Fruhwirth GO, Diocou S, Blower PJ, Ng T, Mullen GED. A whole-body dual-modality radionuclide optical strategy for preclinical imaging of metastasis and heterogeneous treatment response in different microenvironments. *J Nucl Med.* 2014;55:686–694.

13. Jenkins HDB, Roobottom HK, Passmore J, Glasser L. Relationships among ionic lattice energies, molecular (formula unit) volumes, and thermochemical radii. *Inorg Chem.* 1999;38:3609–3620.

14. Trotter J, Whitlow SH. The structures of cæsium and rubidium difluorophosphates. *J Chem Soc Inorg Phys Theor.* 1967;0:1383–1386.

15. McDonald BJ, Tyson GJ. The crystal structure of caesium, ammonium and potassium pertechnetates. *Acta Crystallogr.* 1962;15:87.

16. Krebs B, Hasse KD. Refinements of the crystal structures of $KTcO_4$, $KReO_4$ and OsO_4. The bond lengths in tetrahedral oxoanions and oxides of d^0 transition metals. *Acta Crystallogr B.* 1976;32:1334–1337.

17. Kuntzsch M, Lamparter D, Brüggener N, Müller M, Kienzle GJ, Reischl G. Development and successful validation of simple and fast TLC spot tests for determination of Kryptofix® 2.2.2 and tetrabutylammonium in ^{18}F-labeled radiopharmaceuticals. *Pharmaceuticals.* 2014;7:621–633.

18. Tahara M, Inoue T, Miyakura Y, et al. Cell diameter measurements obtained with a handheld cell counter could be used as a surrogate marker of G2/M arrest and apoptosis in colon cancer cell lines exposed to SN-38. *Biochem Biophys Res Commun.* 2013;434:753–759.

19. Rugh R. The mouse thyroid and radioactive iodine (I-131). *J Morphol.* 1951;89:323–365.

20. Lecat-Guillet N, Ambroise Y. Discovery of aryltrifluoroborates as potent sodium/iodide symporter (NIS) inhibitors. *ChemMedChem.* 2008;3:1207–1209.

21. Demirkaya Ş, Vural O, Dora B, Topçuoğlu MA. Efficacy of intravenous magnesium sulfate in the treatment of acute migraine attacks. *Headache J Head Face Pain.* 2001;41:171–177.

22. Huailei J, Bansal A, Pandey M, et al. Synthesis of ^{18}F-tetrafluoroborate (^{18}F-TFB) via radiofluorination of boron trifluoride and evaluation in a murine C6-glioma tumor model. *J Nucl Med.* 2016; Advance online publication. doi:10.2967/jnumed.115.170894

23. Mendrala AL, Markham DA, Eisenbrandt DL. Rapid uptake, metabolism, and elimination of inhaled sulfuryl fluoride fumigant by rats. *Toxicol Sci.* 2005;86:239–247.

24. Smith GE, Sladen HL, Biagini SCG, Blower PJ. Inorganic approaches for radiolabelling biomolecules with fluorine-18 for imaging with positron emission tomography. *Dalton Trans.* 2011;40:6196–6205.

25. Inkster JAH, Liu K, Ait-Mohand S, et al. Sulfonyl fluoride-based prosthetic compounds as potential 18F labelling agents. *Chem Eur J.* 2012;18:11079–11087.

Figure Legends
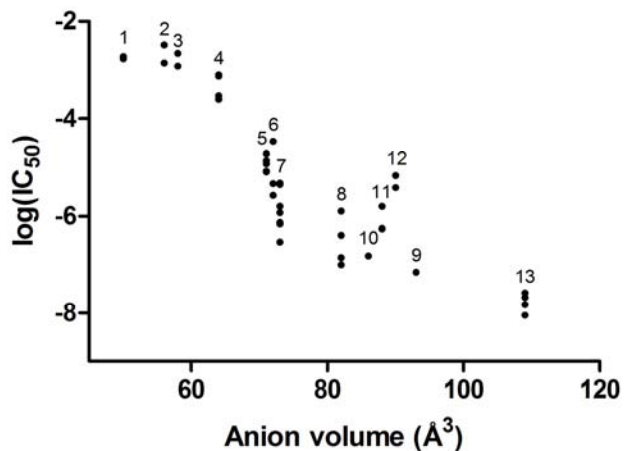
Figure 1. Plot of ionic volume against inhibitory potency (logIC$_{50}$ based on ability to block anion uptake in NIS-expressing cells) for univalent anions examined in this work and other published works (*5,6,7,9,17*). Differing methods, cell lines, probes and counter-ions were used in each study; further details are given in SI Table S1. Numeric labels above each column of data points correspond to particular anions: 1 = CN$^-$, 2 = Br$^-$, 3 = N$_3^-$, 4 = NO$_3^-$, 5 = SCN$^-$, 6 = I$^-$, 7 = BF$_4^-$, 8 = ClO$_4^-$, 9 = TcO$_4^-$, 10 = ReO$_4^-$, 11 = SO$_3$F$^-$, 12 = PO$_2$F$_2^-$, 13 = PF$_6^-$
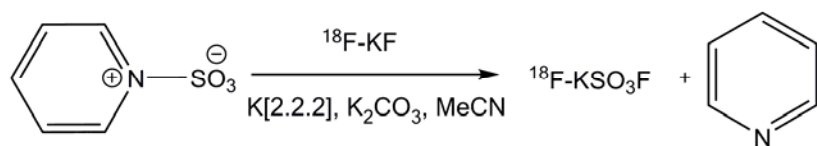
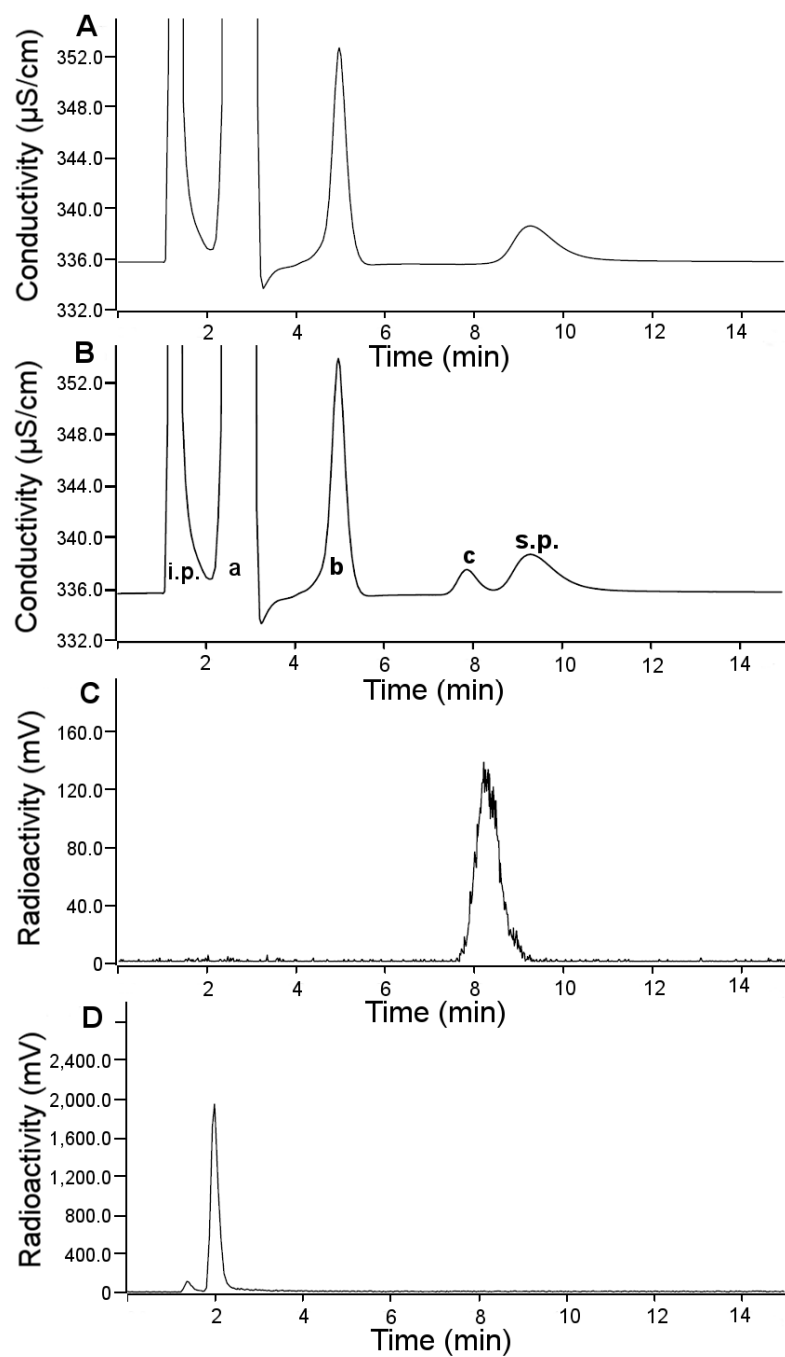Figure 2. Reaction scheme for production of ^{18}F-SO_3F^- from SO_3-pyridine complex

Figure 3. Chromatograms resulting from IC analysis of $^{18}F\text{-}SO_3F^-$: A – Conductivity trace for no-carrier-added $^{18}F\text{-}SO_3F^-$; B – Conductivity trace for co-injection of $^{18}F\text{-}SO_3F^-$ with $^{19}F\text{-}SO_3F^-$ (80 µg/mL): a = Cl^-, b = SO_4^{2-}, c = SO_3F^-, i.p. = injection peak, s.p. = system peak.; C – Radioactivity trace for no-carrier-added $^{18}F\text{-}SO_3F^-$; D – Radioactivity trace for $^{18}F^-$ in H_2O.
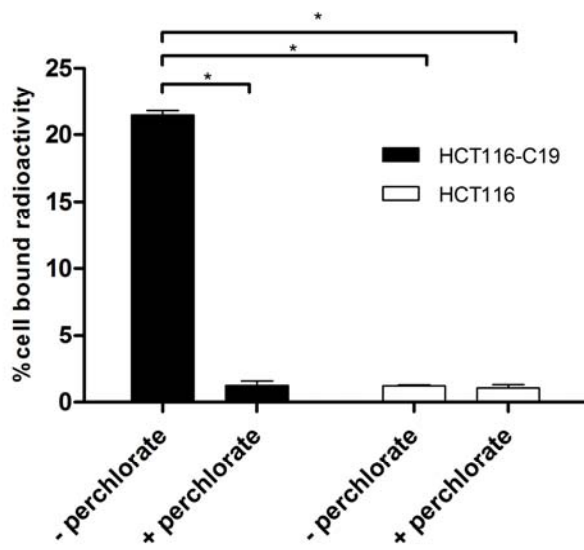
Figure 4. Uptake of ^{18}F-SO$_3$F$^-$ in HCT116-C19 (hNIS-expressing) and HCT116 (hNIS-negative) cell lines in the presence and absence of NaClO$_4$ (20 µM). Error bars represent one SD. Inter-group differences measured by unpaired t-test, * p < 0.00001.

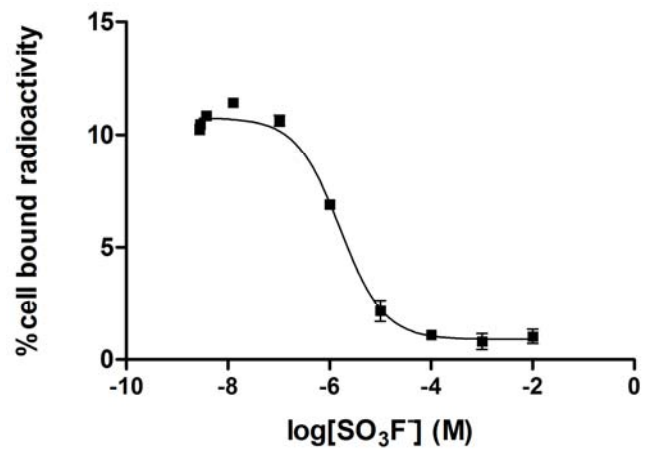Figure 5. Inhibition of uptake of ^{18}F-SO$_3$F$^-$ by ^{19}F-SO$_3$F$^-$ in HCT116-C19 cells. Error bars represent 1 S.D.; IC$_{50}$ = 1.6 μM
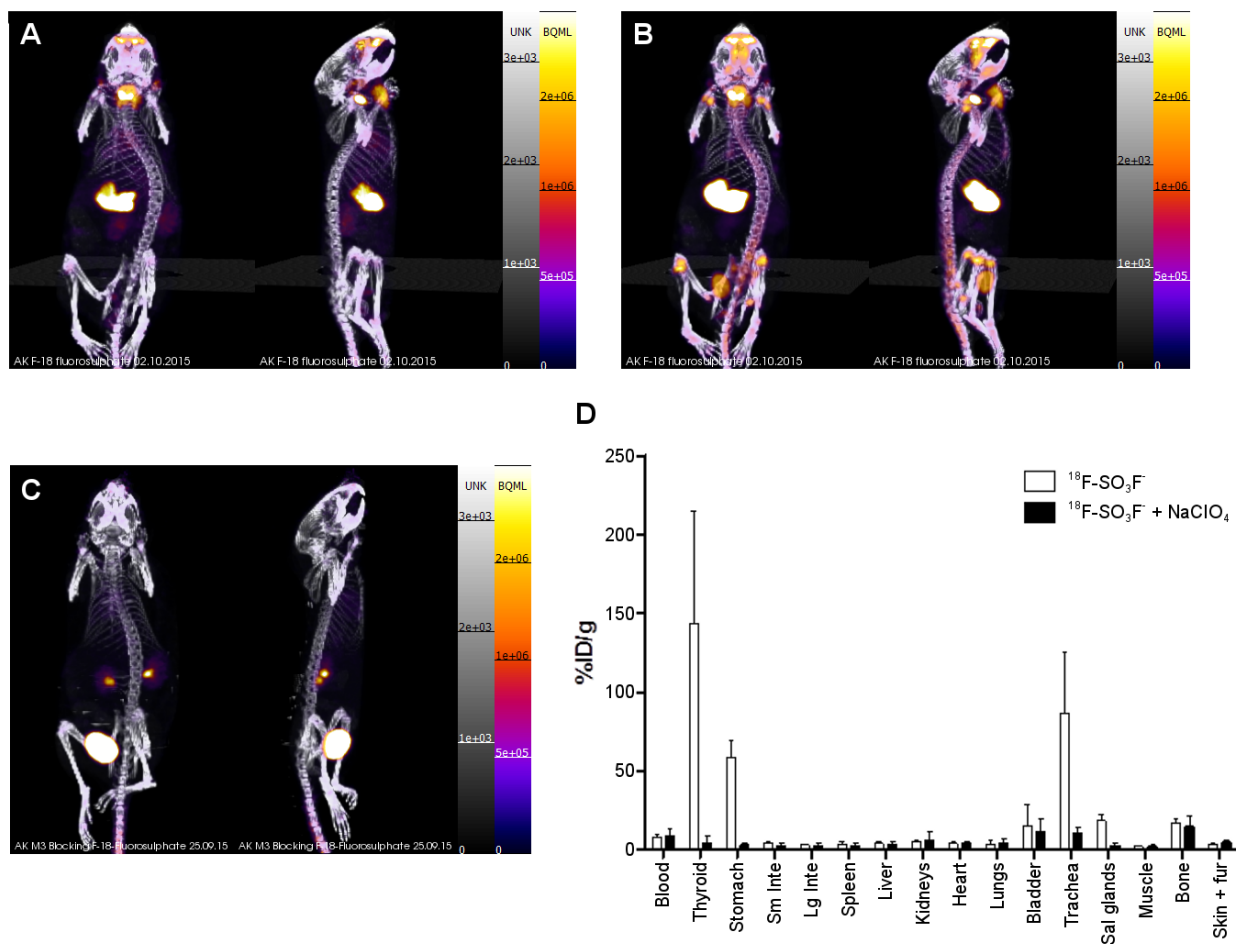
Figure 6. PET/CT images (maximum intensity projections) from anterior and lateral perspectives (A-C) and *ex vivo* biodistribution (D) of BALB/c mice post-injection of ^{18}F-SO$_3$F$^-$. A: 25-30 min post-injection without perchlorate; B: 90-120 min post-injection without perchlorate; C: 25-30 min post-injection in the presence of NaClO$_4$ (250 mg/kg); D: *Ex vivo* biodistribution data at 2.25 h post-injection (n = 3). Uptake measured as injected dose per gram (%ID/g). Error bars represent 1 SD.